Scaling Up Electrodes for Photoelectrochemical Water Splitting: Fabrication Process and Performance of 40 cm^2 LaTiO$_2$N Photoanodes

Stefan Dilger,[b] Matthias Trottmann,[c] and Simone Pokrant*[a]

A scalable process for fabrication of particle-based photoanodes is developed. The electrodes are versatilely made of photocatalytically active semiconductor particles, in this case LaTiO$_2$N, and optionally coated with cocatalysts and protecting components, all immobilized on a conducting substrate. The involved fabrication steps are restricted to scalable processes such as electrophoretic deposition, annealing in air, and dip coating. Special care is taken to ensure efficient charge transport in-between particles and to the substrate by incorporating conducting connectors. By adapting the fabrication steps, the electrode geometrical dimension is increased from the size of a typical lab electrode of 1 to 40 cm^2. The quality of the scale-up process is characterized by comparing the photoanodes in terms of thickness, light-absorption properties, and morphology. For several compositions, the electrochemical performance of both electrode sizes is assessed by measuring the photocurrents and faradaic efficiencies. The comparison revealed a complex upscaling behavior and showed that the photoelectrode size affects performance already on the 0.1 m scale.

Introduction

Harvesting solar energy and its conversion into chemical energy has the potential to contribute substantially towards mitigating the future renewable energy and transportation needs.[1] Direct transformation of solar radiation into hydrogen is considered as an efficient way to produce fuel and chemical feedstock, store energy, and transportation.[1] Among the technologies investigated in this field, photoelectrochemical (PEC) water splitting has seen substantial progress in terms of efficiency enhancement. Conversion efficiencies of up to 18% have been demonstrated for lab-scale devices with typical electrode dimensions of 1 cm^2.[1a, 2] Although PEC technology is still at a very early readiness level, techno–economic studies

pointed out further challenges to achieve economically viable solar hydrogen production. Efficient photocatalysts, around 20% solar-to-hydrogen efficiency (STH), are indispensable but need to be complemented by system cost reductions to achieve competitive production prices for solar hydrogen.[1c] Sathre et al.[3] performed an extensive net energy analysis, modeling and comparing energy consumption of material supply, manufacturing, operation, and end-of-life of a PEC system to the chemical energy of the produced hydrogen. High cell efficiency (20% STH), long life times, and low-energy fabrication processes were identified as predominant criteria to achieve profitable net energy performances for large-scale photoelectrochemical devices.[3] These findings highlight that cell fabrication contributes significantly to the highest energy investment in the life cycle of a potential PEC plant, which is the installation. To move further towards practical implementation, it is mandatory to propose scalable energy- and cost-saving fabrication processes. In addition, these processes need to be tested by fabricating larger scale electrodes, and their performance must be investigated to understand and eventually predict the influence of upscaling on PEC electrodes.

To date there are only a small number of experimental demonstrations of PEC water-splitting electrodes surpassing lab size and addressing the challenges of scale up on a practical level. To distinguish demonstrator size from lab size, we follow the definition of Hankin et al. that one length of the device should be 10 cm or longer to be demonstrator size.[4] Based on this definition, we give an overview of the PEC electrode types which have already achieved demonstrator size. One concept to scale up was put into practice by Turan et al, in which the authors assembled 13 base units to obtain a 64 cm^2 PEC device by integrating 5 cm^2 Si solar cells with Ni foam electro-

[a] Prof. S. Pokrant
Chemistry and Physics of Materials
Paris-Lodron University Salzburg
Jakob-Haringer Str. 2A, 5020 Salzburg (Austria)
E-mail: simone.pokrant@sbg.ac.at

[b] Dr. S. Dilger
Laboratory Materials for Energy Conversion, Empa
Überlandstrasse 129, 8600 Dübendorf (Switzerland)

[c] M. Trottmann
Laboratory Advanced Analytical Technologies, Empa
Überlandstrasse 129, 8600 Dübendorf (Switzerland)

catalysts.[5] Another less labor-intensive approach consists in fabricating larger electrodes. Pareek et al. produced nanorod-like structured 81 cm^2 CdS films by spray pyrolysis on fluorinated tin oxide (FTO), for hydrogen evolution in the presence of a sacrificial agent.[6] Lopes et al. proposed a novel PEC reactor design for 100 cm^2 devices and tested it successfully with WO$_3$ photoanodes. The device was obtained by anodization or blading, and Fe$_2$O$_3$ photoanodes were fabricated by spray pyrolysis.[7] All active layers were deposited on transparent conductive oxides (TCOs). Hankin et al. performed an experimental scale-up study combined with modelling.[4] For this purpose, the authors fabricated 100 cm^2 Sn-doped Fe$_2$O$_3$ photoanodes by spray pyrolysis on Ti foil. These examples demonstrate that scale up of PEC electrodes is possible. However, the question of how to reach demonstrator size electrodes starting from a well-performing lab size electrode has not been addressed experimentally.

In contrast to experimental studies, the question of scale up from lab to demonstrator size has been given some consideration by simulations. Haussener et al.[8] derived design criteria for photoelectrochemical water-splitting systems by numerical modeling. The authors pointed out that the current distribution in large electrodes might be non-uniform owing to potential losses in the current distributing layer. In many practical cases, this layer consists of TCOs and acts as a substrate for the photoelectrochemically active films. This lateral current variation was expected to be less pronounced in the presence of slow kinetics, that is poor catalysts, since there is more time to redistribute the charges. The question of current density distribution in large-scale electrodes has been given specific consideration by Hankin et al. The authors predicted that the effect of electrode geometry and electrode configuration within a photoelectrochemical reactor would affect the performance of photoelectrodes. It was estimated that these effects might be present in electrodes with dimensions in the range of 0.1 m or larger.

In this regards, we present the development of a scalable process for particle-based photoanodes starting from a state-of-the-art lab-sized electrode. We address the question of whether scaling up to demonstrator size changes the photoelectrochemical properties of the electrodes. For this purpose, we fabricated photoanodes with 1 cm^2 (lab size) and 40 cm^2 (demonstrator size) photoactive areas. For several compositions, the photoelectrochemical performance of both photoanode sizes was determined and compared after careful morphological, structural, and optical characterization.

Results and Discussion

LaTiO$_2$N (LTON) was synthesized according to a previous report.[9] Figure S1 (see the Supporting Information) shows the X-ray diffraction (XRD) spectrum of LTON, confirming its single-phase character. Scanning electron microscopy (SEM) images of LTON particles are displayed in Figure 1a. The particles are monocrystalline and brick shaped with an average size of 0.5 to 2 μm in plane and 100–200 nm out of plane, which is in good agreement with a previous report by our group.[10] To
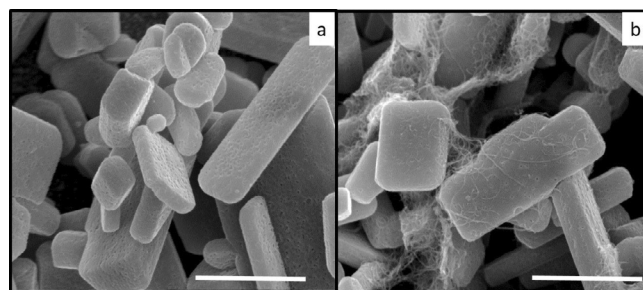
Figure 1. SEM images of a) LTON and b) LTONCNT-composite particles. The scale bar is set to 2 μm.

obtain lab-scale PEC electrodes, LTON powder was deposited on FTO substrates using electrophoretic deposition. Thereafter, the electrodes were dipped in ethanolic solution of TiCl$_4$ and annealed in ammonia flow at 370 °C for 45 min. This step is called necking and was originally proposed for LTON electrodes by Nishimura et al.[11] and later investigated in detail by our group.[9] It serves the following two purposes: (1) Necking guarantees the mechanical stability of the electrode as TiO$_2$ bridges are introduced locally in-between particles and between particles and substrate. (2) Annealing in ammonia leads to partially reduced TiO$_2$, which enables and/or facilitates charge transport in-between particles and between particles and substrate. Electrodes fabricated in this way consist of loosely-stacked micrometer-sized LTON particles held together by nanometer-sized TiO$_2$ bridges (see Figure S2 and S3). Suter et al. studied the 3D structure of LTON electrodes and the location of the TiO$_2$ bridges using focused ion-beam tomography, and confirmed the short-range connectivity introduced by necking.[12] The workflow for the lab-scale electrode preparation is summarized in Figure 2. The photoanodes were denoted by using the following sequence: material-area-annealing condition. For example, LTON-1-N denotes 1 cm^2 photoanodes
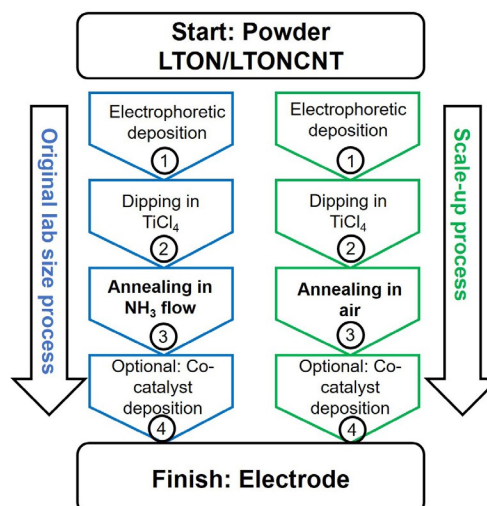
Figure 2. Lab-size process versus scale-up process flow. The difference between lab-size process and scale-up process is restricted to step 3, the annealing condition. The labelling of the electrodes indicates the fabrication route: annealing condition N means lab-size process, annealing condition O means scaled-up process.

made of LTON and annealed in NH_3. The electrodes were optionally coated with cocatalysts and passivation layers (Ta_2O_5, NiO_x, and CoO_x) by scalable dip coating and annealing processes to improve stability and PEC performance. The role of each nanocoating type has been discussed elsewhere.[13] Electrodes with cocatalyst coatings were labeled by adding a suffix -cat to the electrode name. The electrochemical properties of the photoanodes were assessed by measuring the $I–V$ curves under chopped illumination equal to one sun. The photocurrent at 1.23 V versus RHE was used as a performance indicator. LTON-1-N and LTON-1-N-cat could reach photocurrent densities of 65 and 2248 $\mu A\, cm^{-2}$ at 1.23 V (Figure S4). We observed 7% variation upon determining this performance indicator for six LTON-1-N-cat electrodes.[13] This value is a measure for the reproducibility of the lab-scale fabrication process including the nanocoatings.

As expected, the solid-state chemical synthesis of LTON proved to be very suitable for scale-up purposes. Typical batches were in the range even in a laboratory environment, which was enough to cover electrodes with surfaces in the order of several tens of cm^2. The electrophoretic deposition was extended to produce 40 cm^2 electrodes on 10 cm × 5 cm FTO substrates by adapting deposition conditions. The necking step, however, turned out to be the limiting step for scale up of the lab-scale process. The annealing of large electrodes in NH_3 flow to achieve uniform transformation into partially reduced TiO_2 over the entire electrode area turned out to be complex, time consuming, and needed impractical size- and shape-specific adaption of the annealing furnaces. Replacing annealing in NH_3 with scalable annealing in air (see Figure 2) lead to mechanically robust photoanodes, but with diminished activity. Samples annealed in air were denoted with the letter O instead of N. As before, cocatalyst coatings were added and the samples were labeled with the suffix -cat. The photocurrent densities of LTON-1-O and LTON-1-O-cat at 1.23 V were reduced to 19 μA (30% of LTON-1-N) and 319 μA (15% of LTON-1-N-cat), respectively (see Figure S4). This could be credited to the loss of charge-transport character of the partially-reduced TiO_2 necking material (see Figure S3) upon fully oxidizing TiO_2. The fact that insufficient electron transport to the back contact can limit the photocurrent is well known and has been observed before.[14] One way to evaluate charge transport in photoelectrodes consists of comparing photocurrent densities for front and backside illumination (I_{photo}F/B).[15] Electrodes that are not limited by charge transport exhibit front-to-back illumination ratios close to 1, since in this ideal case the location of charge generation does not matter. Ratios larger than 1 indicate that it is favorable if the charges are generated close to the electrode surface. Consequently, for photoanodes the hole diffusion length is shorter than the film thickness, which is the case for hematite.[16] In the opposite case (I_{photo}F/B < 1), a possible interpretation is that electron transport to the back contact is the limiting factor as the charges need to be generated close to the substrate for superior photocurrents. Current ratios of 0.49 and 0.33 were observed at 1.23 V versus RHE for LTON-1-N and LTON-1-O I_{photo}F/B, respectively. These results indicate that LTON-1-O was indeed less able to transport electrons to the back contact than LTON-1-N. In addition, it confirmed the hypothesis that the performance drop in LTON-1-O was attributed to oxidation of the necking material.

To achieve scale up, the charge-transport character of the partially reduced TiO_2 bridges needed to be supplemented by another component. Therefore, we synthesized LTON composites with multi-walled carbon nanotube (CNT) (LTONCNT) using a pH shift reaction (see Figure S2). The crystalline and morphological properties of LTON were not affected by the compound formation using CNTs (Figure S1 and 1b). The LTONCNT hybrid material was electrophoretically deposited on FTO followed by TiO_2 necking through annealing in air at 200 °C for 30 min to obtain mechanical stability. The photocurrents measured for LTONCNT-1-O and LTONCNT-1-O-cat were 307 μA (four times the value of LTON-1-N) and 2287 μA (slightly more than LTON-N-cat), respectively. The I_{photo}F/B ratio for LTONCNT-1-O was found to be 1.5, indicating that all charge-transport issues to the back contact were resolved and that, indeed, charge transport in-between particles and between particles and substrate was improved by CNTs, as also reported previously.[10] In summary, applying the scale-up process presented in Figure 2 to LTONCNT, we obtained comparable or even better results for lab-scale electrodes than with the original LTON lab-scale process.

LTON(CNT)-40-O electrodes, that is, the LTON-40-O and LTONCNT-40-O electrode, were fabricated in analogy to LTON(CNT)-1-O photoanodes by electrophoretic deposition, followed by annealing in air (scale-up process in Figure 2). LTON(CNT) abbreviates LTON and LTONCNT. To guarantee uniform larger-sized electrodes, the LTON(CNT) suspensions were homogenized by replacing the magnetic stirrer with an ultrasonic stirrer during deposition of 40 cm^2 electrodes. The coating of the as-obtained electrodes appeared homogeneous by visual inspection, as demonstrated by the photographs of a 40 and a 1 cm^2 electrode (Figure S5).

To judge whether the scale-up process reproduced 40 cm^2 photoanodes of a comparable quality to 1 cm^2 photoanodes, we performed morphological characterization of both electrode sizes. Considering that the only difference between the 1 cm^2 and the 40 cm^2 scale-up process was the stirring during electrophoretic deposition; film thickness, particle or agglomerate distribution on the substrate, and, most importantly, the optical properties of the photoanodes were selected for comparison. Electrode thickness was measured using profilometry and the results are presented in Figure 3. All electrodes were between 8 and 11 μm thick on average. The 1 cm^2 electrodes were up to 25% thicker than 40 cm^2 electrodes. LTON and especially LTONCNT electrodes showed very noisy profiles owing to the high surface roughness (Figure S6), thereby, hindering a more detailed evaluation and comparison of film thickness. The enhanced roughness of LTONCNT electrodes was connected to the larger size of LTONCNT agglomerates compared to LTON particles, and has been previously observed for lab-size electrodes.[17]
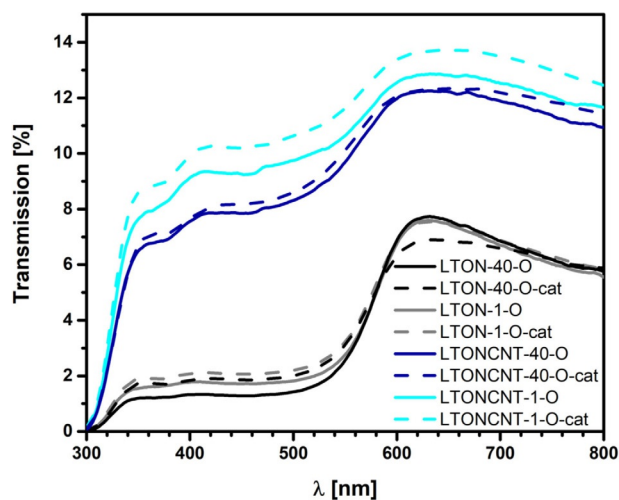
Optical microscopy was used to study electrode morphology. Micrographs of LTON electrodes with 20× magnification showed that the texture of LTON-1-O and LTON-40-O was fun-
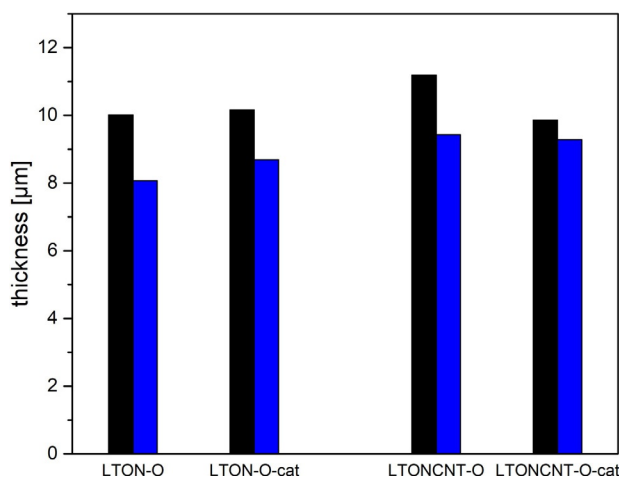
Figure 3. Film thickness of photoanodes fabricated by the scale-up process measured using profilometry. The black columns indicate the average thickness of 40 cm² electrodes versus the 1 cm² electrodes in blue columns. The thickness profiles are displayed in Figure S7.

Figure 4. UV/Vis transmission spectra of LTONCNT-photoanodes fabricated by the scale-up process. LTON spectra are indicated by black (40 cm² electrodes) and grey lines (1 cm² electrodes), whereas LTONCNT spectra are represented by blue (40 cm² electrodes) and cyan lines (1 cm² electrodes). Broken lines label electrodes with cocatalyst coatings.

damentally similar in both cases with or without cocatalysts (Figure S7). LTONCNT optical micrographs were acquired with only 10× magnification because LTONCNT formed larger agglomerates than LTON, as already suggested by the profiles and discussed in Ref.[17] LTONCNT-40-O electrodes showed an even rougher texture than LTONCNT-1-O photoanodes both with and without cocatalysts (Figure S8). A possible interpretation is that a broader size distribution of agglomerates is formed in solution, and subsequently deposited on the 40 cm² electrode owing to the changed stirring conditions provided by ultra sound.

A very important parameter is the ability of photoelectrodes to absorb light, as it directly influences the photoelectrochemical performance. An indirect way to assess this ability consists of measuring the light transmission through the photoanode, assuming that scale up has not changed the light scattering properties of the electrodes. This assumption is reasonable since the building blocks, that is the LTON particles, are same in all photoanodes. LTON and LTONCNT have a band gap of 2.1 eV (590 nm) and absorb in the visible region, whereas FTO absorbs above 320 nm.[17,18] UV/Vis transmission spectra through LTON(CNT) films and FTO substrates are displayed in Figure 4. All spectra showed pronounced losses in transmission below the band gap at 590 nm. Almost no transmission was found below 320 nm, as expected for LTON containing electrodes on FTO substrates. We observed two groups of spectra: spectra belonging to LTON films (black and grey) and spectra coming from LTONCNT electrodes (blue and cyan), Figure 4. LTON spectra were lower in transmission, hence higher in absorption, although the obtained film thickness for LTON electrodes was higher than for LTONCNT electrodes (Figure 3). All LTON electrode spectra were highly similar. Neither scale up nor cocatalyst addition seemed to have a significant effect on the transmission spectra. The narrow optical property range of LTON-electrodes was well supported by the morphological results, in which we found no significant differences in film mor-

phology or thickness as a function of electrode size or cocatalyst addition. Although LTONCNT electrodes were thicker, they transmitted light better than LTON electrodes. Cocatalyst addition had no significant impact on the optical properties. Within the LTONCNT group, there seemed to be a trend that 1 cm² electrodes absorbed slightly less than 40 cm² electrodes. One way to explain these observations relies on taking into account the morphology of the electrode structure on the micrometer scale. The large agglomerates formed by LTONCNT, first in solution and then upon deposition, did not give rise to the same texture in all cases. As discussed above, there were morphological differences between LTON and LTONCNT electrodes and between 1 and 40 cm² LTONCNT electrodes (see Figures S6 and S7). The increased roughness of LTONCNT electrodes, specifically for 40 cm² electrodes, could have led to electrode areas in which the layer of active material is thin and absorbs less light. The white areas/spots in the optical micrographs of LTONCNT electrodes (Figure S8) are indications for the existence of these areas having increased transmission. Hence, it is possible that rough electrodes can show an increased transmission, although the average layer thickness was increased. In summary, for electrodes with complex open structures and textures, the optical properties depend not only on film thickness but also on morphology.

The photoelectrochemical performance of the photoanodes was characterized by measuring the photocurrent density at 1.23 V (vs. RHE) with a Pt wire and Ag/AgCl as the counter and reference electrodes, respectively. For 40 cm² electrodes, a setup was developed which allowed the illumination of about 29 cm² of the electrode surface (see Figure S9 and S10). The electrode was contacted on its shorter side over the entire width of the electrode. The voltammetry scans under back illumination are presented in Figure 5, and under front illumination in Figure S11. The photocurrent densities at 1.23 V (vs. RHE) and the photocurrent ratios of front versus back illumina-

tion are summarized in Table 1. For electrodes with a very low performance, that is LTON-O, we did not find any significant differences between the lab-size electrode and the 40 cm² electrode in terms of photocurrent density or front to back illumination current ratios. As expected, the performance is worse than for LTON-1-N electrodes since charge transport was hindered owing to the oxidized TiO₂ bridges, as discussed above. For the LTON-O-cat configuration, the photocurrent density for the 40 cm² electrode dropped to 54% of that achieved with 1 cm² electrode. Nevertheless, LTON-40-O-cat photocurrent densities were higher than for the LTON-40-O elec-

trode over the entire potential range because of cocatalyst addition. Charge transport properties stayed at comparably low values, similar to LTON-O, for the same reasons. LTOCNT electrodes reached photocurrent densities comparable to LTON-O-cat electrodes. Again, a drop of photocurrent density was observed for large photoelectrodes in the same order of magnitude, in this case 48% compared to the performance of the lab-size electrode. Electron transport was improved owing to

Table 1. Photoelectrochemical performance of LTON(CNT) of 1 cm² (left) and 40 cm² electrodes (right). J_{Photo} indicates the photocurrent density at 1.23 V (vs. RHE). Electrodes fabricated using the scale-up process are labeled with O, whereas electrodes from the lab-scale process contain N in the sample name. The corresponding voltammetry scans are displayed in Figures 5 and S10.

Sample (1 cm²)	I_{Photo}F/B	J_{Photo} [µA cm⁻²]	J_{Photo} [µA cm⁻²]	I_{Photo}F/B	Sample (40 cm²)
LTON-1-N	*0.5*	*65*	–	–	
LTON-1-O	0.3	19	33	0.3	LTON-40-O
LTON-1-O-cat	0.3	319	172	0.4	LTON-40-O-cat
LTONCNT-1-O	1.5	307	146	0.8	LTONCNT-40-O
LTONCNT-1-O-cat	1.0	2287	563	0.9	LTONCNT-40-O-cat

the presence of MWCNTs, reaching ideal values of around 1, and in the case of 1 cm² electrodes even above 1. The best performance was obtained for LTONCNT-O-cat electrodes with photocurrent densities of 2.29 mA cm⁻² for the lab size electrode and 0.56 mA cm⁻² for the 40 cm² electrode. Here, scale up lead to the largest drop since only 25% of the original photocurrent density was retained. The front to back illumination current ratios were similar for both electrode sizes. In summary, scale up seemed to mainly affect photocurrent density, for which the reduction was directly correlated to the photocurrent density of the lab-size electrode.

It was necessary to rule out that chemical reactions on the electrodes had changed because of scale up as significant photocurrent losses were observed for large-scale electrodes. Therefore, we measured the faradaic efficiencies of the 40 cm² electrodes (Figure 6). Faradaic efficiencies of 86% to 90% were obtained for the hydrogen evolution reaction and the oxygen evolution reaction, respectively; additionally, some N₂ evolution was also observed. These observations and the faradaic efficiencies are typical for LTON electrodes and have been previously described by our group (83–84%)[17] and in literature (80–76% and 93–92%)[19] for lab-size electrodes. The efficiency losses have been mainly attributed to back reactions and partially to corrosion. Although, clearly some corrosion took place in LTON electrodes as suggested by the gradual reduction in current over time (Figure 6). This behavior was similar for small and large electrodes. Therefore, the observed photocurrent losses for large-scale electrodes could not be connected to any clear changes of the chemical reactions on the electrodes.

The morphological and/or optical differences of LTON(CNT) thin films on FTO substrates could be another potential source for photocurrent losses during scale up. However, LTON-O-cat showed very similar optical properties for lab-scale and demonstrator-size electrodes. Nevertheless, a significant drop in photocurrent was observed. For LTONCNT-O-(-cat) electrodes the situation was even opposite to expectations. Lab-size electrodes transmitted more light than large-scale electrodes but exhibited higher photocurrents. Hence, we concluded that the subtle optical and morphological differences between the various electrodes were not decisive for the pronounced photocurrent density variations.

A critical feature for particle-based electrodes is charge transport from the active site to the back contact, as already mentioned. However, the front-to-back illumination current
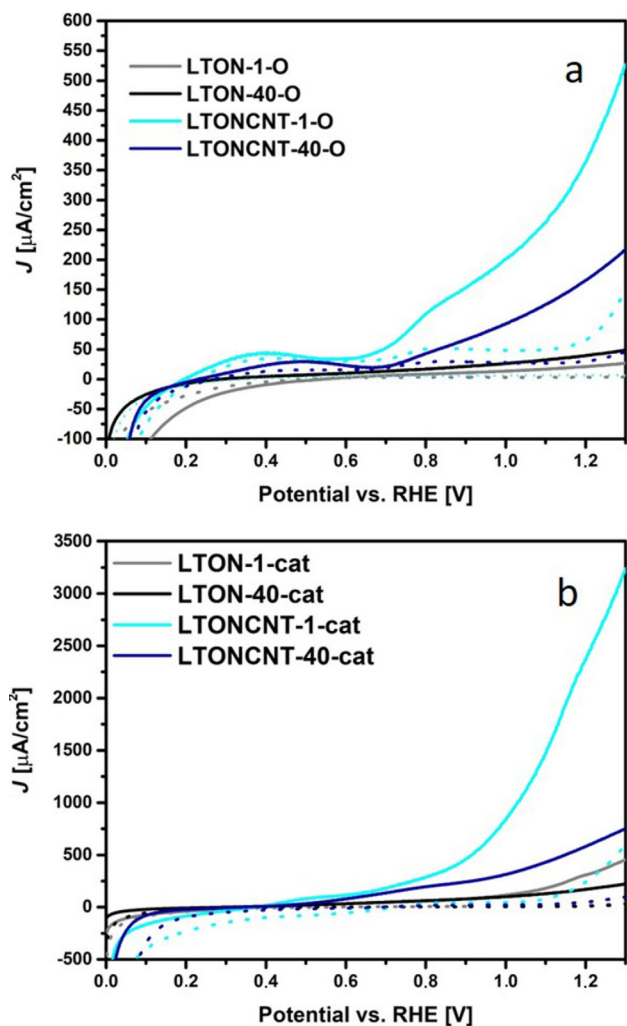
Figure 5. J–V curves of LTON and LTONCNT electrodes in back illumination a) without and b) with cocatalysts. Dark currents were added as dotted lines.
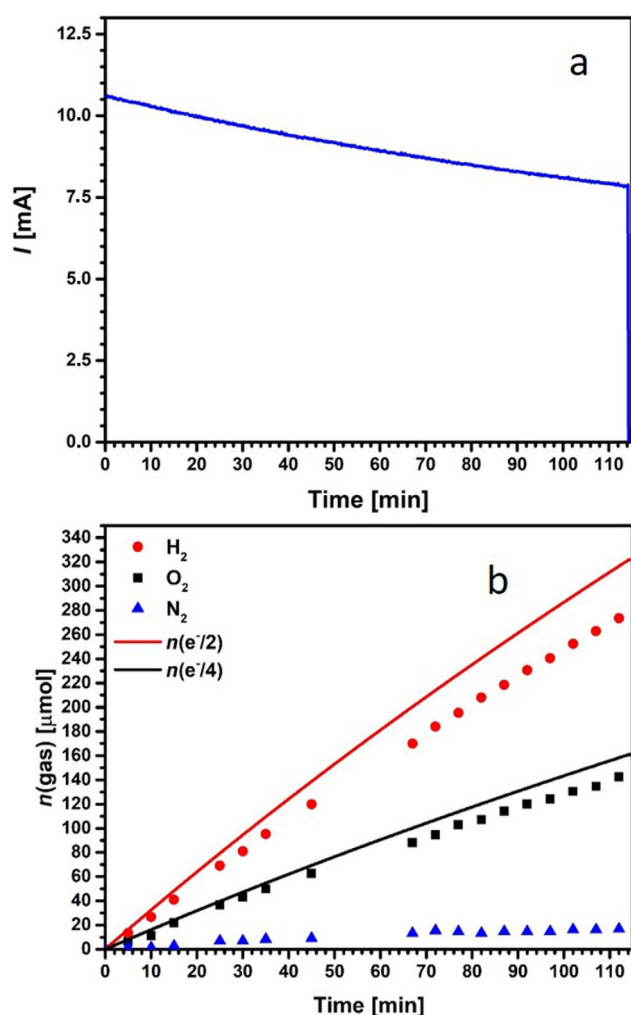
Figure 6. a) Chronoamperometric measurement and b) oxygen and hydrogen evolution of LTONCNT-40-O-cat. The charges $n(e^-/2)$ and $n(e^-/4)$ were obtained by integrating the current I over time and dividing it by 2 and 4, respectively.

ratios listed in Table 1 indicate similar behavior for all electrode types before and after upscaling, with the exception of LTONCNT. The measured ratio for the large-scale LTONCNT-40-O electrode (0.8) was smaller than for the lab-size electrode LTONCNT-1-O (1.5), but still indicates good transport properties, which is superior to LTON-1-N. Therefore, it is unlikely that charge transport to the back contact is responsible for the drop-in photocurrent after scale up. However, in large-scale electrodes lateral transport to the electrical contact point or line could be an issue. Since the demonstrator-sized FTO substrate collects charge over a larger area and transports it over longer distances than lab-size electrodes, the FTO resistivity might be a limiting factor. Indeed, upon decreasing the FTO resistivity from 15 to 7 $\Omega\,sq^{-1}$, we obtained a current density of 680 $\mu A\,cm^{-2}$ for LTONCNT-40-O-cat electrodes, which is an improvement of about 100 $\mu A\,cm^{-2}$ (see Figure S12). However, we still recovered only 30% photocurrent density of the lab-size electrode.

To identify potential reasons for the reduced photocurrent density induced by scale up, we relied on device modeling re-

sults obtained mainly from demonstrator-size hematite photoanodes.[4, 20] The size of the modeled device (0.1 m × 0.1 m) was comparable to our electrodes (0.1 m × 0.04 m). The authors studied various electrode geometries and positions in the reactor to analyze the influence of ion-diffusion path lengths on the photoelectrochemical performance. They concluded that this effect was minimal in electrolytes with a high ionic strength.[4] As this was the case in our experiments (0.1 M Na_2SO_4 and NaOH at pH = 13.6), ion-diffusion path lengths appear to be secondary for device performance in our conditions, and were excluded as a potential reason for the substantial performance drop. Another result of the 2D study performed by Hankin et al. was that the performance of electrodes with dimensions larger than 0.1 m were drastically affected by variations in the spatial distribution of potential, and subsequently of the local photocurrent densities over the electrode length, assuming only one electrical contact point at the electrode end.[4] The higher the local photocurrent was at the contact point, that is the better the photoelectrode performed potentially, the stronger the local photocurrent dropped over device length. For example, the authors calculated a drop of 13% for 10 cm long hematite electrodes with local photocurrent densities of 0.27 $mA\,cm^{-2}$ at 1.5 V (vs. RHE) at the contact point, whereas a drop of 78% was predicted for initial values of 4 $mA\,cm^{-2}$. The measurement setup used for photocurrent density determination mimicked this 2D study very well for 10 cm electrode lengths, as we contacted the short side of the electrode over the entire length. Quantitative comparison with LTON(CNT) electrodes was not possible as the model was set up for a different material. In addition, the experimentally measured average photocurrent density corresponds to the modelled local photocurrent density integrated over the entire length. However, the order of magnitude of photocurrent losses is similar to our experimental results for LTON(CNT) electrodes. Another potential reason for photoelectrode performance reduction could be blocking of active sites and/or back reactions because of sticking gas bubbles. Figure S13 includes a movie of oxygen evolution on a LTONCNT-40-O-cat photoanode. In the lower part of the electrode, some bubbles were not moving during the time of movie acquisition. Simulations performed for hematite suggested that efficiency reduction because of adsorbed gases was relevant exclusively at very low photocurrents, that is, two to three orders of magnitude smaller than the experimental LTON(CNT) photocurrent densities.[20] Otherwise, the gases appeared to desorb by bubble evolution. Consequently, electrode performances were not affected significantly. Therefore, we think that the sticking of oxygen gas bubbles at the lower end of the LTONCNT-40-O-cat photoanode provides further indications for the low local photocurrent densities far away from the contact point. However, it seems unlikely that this is the origin of the massive performance loss observed for demonstrator-size electrodes. Based on the analysis presented here, we propose that the performance of LTON(CNT) electrodes was strongly affected by electrode length already in the range of 0.1 m. The reason is that local photocurrent densities drop quickly with distance from the electrical contact point at which the bias is applied.

The effect is stronger for better-performing photoanode configurations. Collaboration with modeling and simulations seem to be essential to take the right approach for scale up in terms of electrode size and geometry.

Conclusions

By adapting electrode fabrication, a truly scalable process was developed for production of particle-based LaTiO$_2$N (LTON) electrodes. The fabrication steps were restricted to electrophoretic deposition, annealing in air, and dip coating. To ensure charge conductivity from the active layer to the substrate, an alternate composite material LTONCNT was used for electrode deposition. In addition, cocatalyst nanolayers were deposited optionally. The geometrical electrode dimensions were increased from the size of a typical lab electrode (1 cm^2) to demonstrator size (40 cm^2). Characterization of electrode thickness, morphology, and optical properties revealed good reproducibility for LTON electrodes and minor differences for LTONCNT electrodes, which were attributed to scale up. The complex 3D structure of particle-based electrodes needs to be taken into account to correctly associate the optical properties to electrode thickness, morphology, and texture, as in Ref [12]. Special attention should be paid to potential inhomogeneities in the CNT network, which could be decisive for LTON activity in LTONCNT samples. Photoelectrochemical performance evaluation showed that scale up did not affect faradaic efficiency, however, photocurrent densities were strongly affected. Photocurrent density losses up to 75% were observed as a function of the electrode composition. Electrode configurations with high lab-size photocurrent densities showed more pronounced losses, that is, from 2287 to 563 µA cm^{-2}. Therefore, we can conclude that LTON(CNT) electrodes at demonstrator size of 40 cm^2 were already clearly affected by size-related performance changes. Insufficient charge transport by the substrate over longer distances could be identified as a source of performance loss and about 5% of the photocurrent density could be recovered by doubling the substrate conductivity. To fully understand the origin of the remaining 70% photocurrent density loss simulations are essential. The simulated rapid decay of local photocurrent densities as a function of distance from the electrical contact point, at which the bias is applied, was proposed as a potential explanation. Collaboration with predictive modelling is planned[21] to find better suited electrode sizes, reactor geometries and/or substrate properties. In the view of potential implementation of PEC devices, the complexity of electrode scale-up should not be underestimated keeping in mind that high performing electrodes potentially need a tighter network of bias contact points to maintain their performance at larger scale.

Experimental Section

Electrode preparation

Solid-state synthesis: LaTiO$_2$N (LTON) and LTON/multiwalled carbon nanotube (MWCNT) composite materials (LTONCNT) with 1% MWCNT content were synthesized as previously reported.[10] Photoanodes were fabricated by electrophoretic deposition of the powders with 1 and 40 cm^2 active areas, respectively, similar to a previously reported process.[10] Fluorine-doped tin oxide on glass (FTO) was purchased from Solaronix (TCO22-15 having resistivity of 15 Ω sq^{-1}) in two sizes 2.5×1.0 and 10×5 cm^2, which served as substrates. If indicated, TCO11-7 with resistivity of 7 Ω sq^{-1} was used instead. FTO substrates were thoroughly washed with soap, distilled water, and acetone in an ultrasonic bath, and were stored in isopropanol. A solution of I$_2$ (Sigma–Aldrich, 99.8%, 12.5 mg) in acetone (Merck, pro analysis, 62 mL) was prepared. LTON and LTONCNT suspensions were prepared using the above solution with a ratio of 0.73 mg of material per 1 mL of acetone/I$_2$ solution by ultrasonication. The oxynitride (composite) particles were positively charged by adsorption of protons generated from the reaction between I$_2$ and C$_3$H$_6$O. Two FTO substrates with conductive sides facing each other were immersed into the suspension at a distance of 6.5 mm. An electric field was applied by connecting the FTO slides to a voltage supply set to 20 V, causing the positively charged particles to migrate to the anode.

1 cm^2 electrodes: The LTON and LTONCNT particles were deposited for 210 s under magnetic stirring, at 400 rpm for 10 s after each minute, to keep the particles dispersed. Necking was performed by dipping the coated electrodes into a 0.2 M solution of TiCl$_4$ in ethanol followed by annealing in NH$_3$ flow (100 mL min^{-1}) for 45 min at a temperature of 370 °C, or in air for 30 min at a temperature of 200 °C.

40 cm^2 electrodes: Electrophoretic deposition over the large electrode took place for 210 s in the presence of an ultrasonic stirrer (Bandelin, SONOPLUS, HD 3100, 10% Amplitude). Post-treatments to increase the mechanical stability through TiO$_2$ bridges between particles were performed by dipping the electrodes into a 0.2 M solution of TiCl$_4$ in ethanol for 10 s followed by drying at room temperature and annealing in air for 30 min at 200 °C.

Functional cocatalyst coatings of Ta$_2$O$_5$, NiO$_x$, and CoO$_x$ were applied by dip coating followed by annealing as previously described.[10,13,17] The depositions proceeded as follows: TiO$_2$-necked electrodes were dipped into 0.2 M solution of TaCl$_5$ in ethanol for 10 s and subsequently dried at room temperature. Afterwards, the electrodes were annealed in air for 30 min at 200 °C. The electrodes were then dipped into a 50 mM solution of Ni(NO$_3$)$_2$ in ethanol for 20 s, dried at room temperature and annealed in air at 200 °C for 10 min. Finally, the electrodes were dipped into a 50 mM solution of Co(NO$_3$)$_2$ in ethanol for 20 s, dried at room temperature and annealed in air at 150 °C for 10 min.

Structural and optical characterization

XRD patterns were acquired from 10° to 80° (2θ) with an angular step interval of 0.008° using a PANanalytical X'Pert PRO θ-2θ scan system (Bragg–Brentano geometry) equipped with a Johansson monochromator (Cu$_{K\alpha1}$ radiation, 1.540598 Å) and an X'Celerator linear detector. A FEI NovaNanoSEM equipped with an immersion lens detector was used to study LTON and the respective electrodes. A 10 kV beam acceleration voltage was used. Profilometry measurements were performed on a Bruker DektakX with a 1 µm 60° tip and an applied contact weight of 1 mg. UV/Vis transmission spectra of LTON and LTON/MWCNT electrodes were acquired over a spectral range of 400–800 nm (2.7–1.5 eV) using a UV/Vis/NIR spectrophotometer (UV-3600 Shimadzu) in transmission mode. Optical microscopy images were acquired on an Axioplan microscope (Zeiss).

Photoelectrochemical characterization

Photoelectrochemical measurements were conducted in a three-electrode configuration with the LTON(CNT) films as the working electrode, an Ag/AgCl reference electrode (in 3 M KCl), and a Pt wire as counter electrode. An aqueous solution of 0.1 M Na_2SO_4 with pH 13.40, adjusted by adding solid NaOH, was used as the electrolyte. A 300 W Xe lamp (Lot Oriel) equipped with an AM1.5G filter with an intensity of 100 mW cm^{-2} calibrated with a Si photodiode was used as the light source. Current densities J were acquired on a VersaSTAT 4 potentiostat with a scan rate of 10 mV s^{-1}. The irradiated area was 0.57 cm^2 for 1 cm^2 electrodes and about 29 cm^2 for 40 cm^2 electrodes (Figures S9 and S10), respectively. Voltammetry scans were performed under illumination, in dark, in back illumination (through the FTO glass), and front illumination conditions. Photocurrents were calculated from these data by subtracting the dark current from the current measured under illumination. Alternatively, chopped illumination was used.

Gas chromatography was used to directly measure the water splitting performance of the electrodes. Gas evolution of H_2, O_2, and N_2, a possible product of photocorrosion of LTON, were measured using an Inficon gas chromatograph attached to a three-electrode custom built air-tight cell with an Ag/AgCl reference electrode and a Pt-spiral counter electrode. The gas chamber was evacuated and flushed with Ar ten times prior to measurement. The electrodes were dipped in an aqueous solution of 0.1 M Na_2SO_4 with pH 13.40, adjusted by adding NaOH. Chronoamperometric measurements were performed with the same setup as described above.

Acknowledgements

Conflict of interest

The authors declare no conflict of interest.

[1] a) S. Y. Tee, K. Y. Win, W. S. Teo, L.-D. Koh, S. Liu, C. P. Teng, M.-Y. Han, *Adv. Sci.* **2017**, *4*, 1600337; b) B. A. Pinaud, J. D. Benck, L. C. Seitz, A. J. Forman, Z. B. Chen, T. G. Deutsch, B. D. James, K. N. Baum, G. N. Baum, S. Ardo, H. L. Wang, E. Miller, T. F. Jaramillo, *Energy Environ. Sci.* **2013**, *6*, 1983 – 2002; c) M. R. Shaner, H. A. Atwater, N. S. Lewis, E. W. McFarland, *Energy Environ. Sci.* **2016**, *9*, 2354 – 2371.
[2] a) J. W. Ager, M. R. Shaner, K. A. Walczak, I. D. Sharp, S. Ardo, *Energy Environ. Sci.* **2015**, *8*, 2811 – 2824; b) K. Zhang, M. Ma, P. Li, D. H. Wang, J. H. Park, *Adv. Energy Mater.* **2016**, *6*, 1600602.
[3] R. Sathre, J. B. Greenblatt, K. Walczak, I. D. Sharp, J. C. Stevens, J. W. Ager, F. A. Houle, *Energy Environ Sci* **2016**, *9*, 803 – 819.
[4] A. Hankin, F. E. Bedoya-Lora, C. K. Ong, J. C. Alexander, F. Petter, G. H. Kelsall, *Energy Environ. Sci.* **2017**, *10*, 346 – 360.
[5] B. Turan, J.-P. Becker, F. Urbain, F. Finger, U. Rau, S. Haas, *Nat. Commun.* **2016**, *7*, 12681.
[6] A. Pareek, R. Dom, P. H. Borse, *Int. J. Hydrogen Energy* **2013**, *38*, 36 – 44.
[7] T. Lopes, P. Dias, L. Andrade, A. Mendes, *Sol. Energy Mater. Sol. Cells* **2014**, *128*, 399 – 410.
[8] S. Haussener, C. Xiang, J. M. Spurgeon, S. Ardo, N. S. Lewis, A. Z. Weber, *Energy Environ. Sci.* **2012**, *5*, 9922 – 9935.
[9] S. Landsmann, A. E. Maegli, M. Trottmann, C. Battaglia, A. Weidenkaff, S. Pokrant, *ChemSusChem* **2015**, *8*, 3451 – 3458.
[10] S. Pokrant, S. Dilger, S. Landsmann, *J. Mater. Res.* **2016**, *31*, 1574 – 1579.
[11] N. Nishimura, B. Raphael, K. Maeda, L. Le Gendre, R. Abe, J. Kubota, K. Domen, *Thin Solid Films* **2010**, *518*, 5855 – 5859.
[12] S. Suter, M. Cantoni, Y. K. Gaudy, S. Pokrant, S. Haussener, *Sustainable Energy Fuels* **2018**, *2*, 2661 – 2673.
[13] S. Landsmann, Y. Surace, M. Trottmann, S. Dilger, A. Weidenkaff, S. Pokrant, *ACS Appl. Mater. Interfaces* **2016**, *8*, 12149 – 12157.
[14] F. F. Abdi, R. van de Krol, *J. Phys. Chem. C* **2012**, *116*, 9398 – 9404.
[15] R. Van de Krol, M. Grätzel, *Photoelectrochemical Hydrogen Production*, Springer, New York, **2012**, pp. 96 – 97.
[16] Y. Liang, C. S. Enache, R. van de Krol, *Int. J. Photoenergy* **2008**, 739864.
[17] S. Dilger, S. Landsmann, M. Trottmann, S. Pokrant, *J. Mater. Chem. A* **2016**, *4*, 17087 – 17095.
[18] A. E. Maegli, S. Pokrant, T. Hisatomi, M. Trottmann, K. Domen, A. Weidenkaff, *J. Phys. Chem. C* **2014**, *118*, 16344 – 16351.
[19] a) S. Akiyama, M. Nakabayashi, N. Shibata, T. Minegishi, Y. Asakura, M. Abdulla-Al-Mamun, T. Hisatomi, H. Nishiyama, M. Katayama, T. Yamada, K. Domen, *Small* **2016**, *12*, 5468 – 5476; b) J. Feng, W. Luo, T. Fang, H. Lv, Z. Wang, J. Gao, W. Liu, T. Yu, Z. Li, Z. Zou, *Adv. Funct. Mater.* **2014**, *24*, 3535 – 3542.
[20] F. E. Bedoya-Lora, A. Hankin, G. H. Kelsall, *J. Mater. Chem. A* **2017**, *5*, 22683 – 22696.
[21] Y. K. Gaudy, S. Dilger, S. Landsmann, U. Aschauer, S. Pokrant, S. Haussener, *J. Mater. Chem. A* **2018**, *6*, 17337 – 17352.